Angular anisotropy of the Kr $3d^{-1}_{3/2,5/2}5p \rightarrow 4p^{-2}5p$ resonant Auger decay studied by utilizing the Auger resonant Raman effect

H. Aksela, J. Jauhiainen, E. Nõmmiste, and S. Aksela
Department of Physical Sciences, University of Oulu, Linnanmaa, FIN-90570 Oulu, Finland

S. Sundin, A. Ausmees, and S. Svensson
Department of Physics, Uppsala University, Box 530, S-75125 Uppsala, Sweden
(Received 28 February 1996)

The anisotropy of the resonant Auger decay of the photoexcited Kr $3d^{-1}_{3/2,5/2}5p$ states has been studied by comparing the new high-resolution experimental results with the multiconfiguration Dirac-Fock calculations. The measurements were made with very high photon and electron energy resolutions in the Auger resonant Raman mode giving ''subnatural'' linewidths of $\sim$ 35 meV, which has enabled us to resolve the fine structures in detail. Comparison with high-quality experimental results allows us to confirm the roles of exchange interaction as well as initial- and final-state interactions in the theoretical description of the angular anisotropy of the resonant Auger transitions. [S1050-2947(96)08507-1]

PACS number(s): 32.80.Hd, 32.80.Fb

I. INTRODUCTION

When an excited state with an inner shell vacancy decays via an Auger transition, the angular distribution of emitted electrons may be anisotropic. Within the framework of a two-step model, the angular dependence of Auger emission is governed by the product of two factors, the alignment parameter of the intermediate state and the anisotropy parameter of the Auger decay. The calculated results for the anisotropy of resonant Auger decay have been found [1] to be very sensitive to the details of the theory to account for the atomic structure. The spectator-core interaction that furthermore affects the strength of final ionic-state configuration interaction (FISCI) [1–3] gives rise to pronounced effects in the angular distribution of resonant Auger decay.

In earlier experiments, it has usually not been possible to resolve separate Auger electron lines corresponding to transitions between well-defined initial and final states. Recent developments in the areas of high-intensity undulator sources as well as high-resolution monochromators and electron spectrometers with rotational capabilities have made it possible for us to measure the angular distribution of resonant Auger electrons with higher accuracy than before. Especially advantageous is the use of Auger resonant Raman effect [4], which allows one to diminish the linewidths substantially by exciting the resonance with a photon band that is much narrower than the lifetime-broadened absorption resonance. As a result, the fine-structure splitting caused by the coupling of the angular momenta of the final double-hole core and the spectator electron can be resolved. Higher accuracy of experiment, especially concerning the angular anisotropy, allows us to make a more careful comparison between experiment and theory. This makes it possible to confirm the roles of various correlation effects in describing the experiment.

The main focus of this work is to study the angular anisotropy of the Kr $3d^{-1}_{3/2,5/2}5p \rightarrow 4p^{-2}5p$ resonant Auger transitions by comparing the new experimental results with the multiconfiguration Dirac-Fock (MCDF) calculations. Present experimental anisotropy parameters are also compared with earlier results of lower resolution measurements [5,6] in order to find out if the high-resolution measurements can clarify the discrepancies between the earlier studies. The role of angular anisotropy as compared to partial decay rates and energy splitting as a tool to test the theory is also discussed.

II. CALCULATIONS

We treat the resonant Auger decay as a two-step process in which the interference between the resonant and direct ionization channels is ignored. The angular distribution of Auger electrons produced in photoabsorption by a beam of linearly polarized photons can be written as

$$\frac{dW_{i\rightarrow f}(\theta)}{d\omega} = \frac{W^T_{i\rightarrow f}}{4\pi}[1+\beta P_2(\cos\theta)]. \tag{1}$$

Here $W^T_{i\rightarrow f}$ is the angle-integrated Auger decay rate between intermediate and final ionic states having total angular momenta J_i and J_f, respectively. θ is the angle between the direction of the Auger electrons and the polarization vector and $P_2(\cos\theta)$ is the second Legendre polynomial. The angular distribution parameter $\beta = \alpha_2 \mathcal{A}_{20}$, where $\mathcal{A}_{20}$ is the alignment of the excited state. In photoexcitation from the ground state $J=0$ to the $J_i=1$ state using linearly polarized photons, the substates with only one projection $M_i=0$ may be populated, and the alignment parameter $\mathcal{A}_{20}$ has an energy-independent value of $-\sqrt{2}$.

Coefficient α_2 is the Auger decay anisotropy parameter which depends on the contributing Auger transition amplitudes and their relative phases. In order to visualize this dependence, the anisotropy parameter α_2, given for instance by Eq. (A27) of Ref. [7], may be rewritten as

$$\alpha_2 \sim N^{-1} \sum_{\kappa,\kappa'} B_{\kappa,\kappa'} A_\kappa A_{\kappa'} \cos(\triangle_{\kappa\kappa'}). \tag{2}$$

TABLE I. Experimental and calculated kinetic energies and angular anisotropy parameters $\beta=\alpha_2 A_{20}$ for Kr $3d_{5/2}^{-1}5p\rightarrow 4p^{-2}5p$ Auger transitions. F and FE indicate the results obtained using final-state orbitals and excluding or including, respectively, the exchange for the continuum electron. IE indicates the values obtained using initial-state orbitals with exchange.

Final ionic state		Line	Energy (eV)		β				
Parent	Term	in expt.	Calc.	Expt.	F	FE	IE	Chen [3]	Expt.
$4p^4(^3P)5p$	$^4P_{5/2}$	1	60.953	60.597	−0.999	−0.994	−0.996	−0.999	−0.97±0.03
	$^4P_{3/2}$	2	60.891	60.552	1.019	1.057	1.029	1.003	0.68±0.13
	$^4D_{7/2}$	3	60.723	60.367	−0.794	−0.463	−0.533	−0.808	−0.54±0.06
	$^4P_{1/2}$	3	60.688	60.367	−0.208	−0.210	0.422	0.424	
	$^2D_{5/2}$	4	60.665	60.331	−0.999	−0.991	−0.996	−0.999	−0.95±0.02
	$^2D_{3/2}$	5	60.341	60.045	0.797	0.804	0.902	0.822	1.07±0.04
	$^2P_{1/2}$	6	60.229	59.955	0.737	0.395	0.841	0.850	0.7 ± 0.2
	$^4D_{5/2}$	7	60.177	59.830	−0.766	−0.771	−0.302	−0.768	
	$^2P_{3/2}$	8	60.120	59.827	−0.922	−0.860	0.499	0.382	0.07±0.03
	$^2P_{1/2}$	9	60.170	59.824	1.056	1.107	1.005	1.034	
	$^4S_{3/2}$	10	59.962	59.631	−0.727	−0.685	−0.981	−0.899	−0.12±0.04
	$^4D_{3/2}$	11	59.858	59.597	0.930	0.847	0.861	0.949	1.04±0.05
	$^4D_{1/2}$	12	59.807	59.551	0.710	0.270	0.859	0.891	0.73±0.07
$4p^4(^1D)5p$	$^2F_{5/2}$	13	58.700	58.706	−0.852	−0.796	−0.794	−0.857	−0.8 ± 0.2
	$^2F_{7/2}$	14	58.641	58.641	0.026	0.280	0.218	0.049	0.20±0.06
	$^2P_{3/2}$	15	58.427	58.579	0.226	0.290	0.112	0.297	0.64±0.08
	$^2D_{3/2}$	16	58.280	58.332	−0.979	−0.891	−0.109	−0.290	
	$^2P_{1/2}$	17	58.137	58.326	1.274	1.204	1.262	1.239	0.24±0.07
	$^2D_{5/2}$	18	58.305	58.317	−0.859	−0.805	−0.794	−0.861	
$4p^4(^1S)5p$	$^2P_{1/2}$	19	56.689	56.339	−0.013	−0.253	1.045	0.976	
	$^2P_{3/2}$	20	56.678	56.256	0.836	0.840	0.807	0.839	0.86±0.09

In Eq. (2), $B_{\kappa\kappa'}$ is a geometrical factor, $A_\kappa=|\langle\psi_i||H_I||\Phi_{\Gamma E}^-\rangle|$ is the absolute value of the transition amplitude, where $|\psi_i\rangle$ stands for the intermediate core-hole atomic state, and $|\Phi_{\Gamma E}^-\rangle$ for the final continuum state. $\triangle_{\kappa\kappa'}$ is the phase difference between channels having Auger electron quantum numbers κ and κ' $[\kappa=(l-j)(2j+1)]$, where l and j are the orbital and total angular momenta of the continuum electron. The normalization factor is given by $N=\Sigma_\kappa|A_\kappa|^2$. A detailed theoretical analysis of the anisotropy of Auger emission within the multiconfiguration Dirac-Fock formalism is given in Ref. [7].

In most experiments so far, the energy resolution has not been sufficient to resolve the transitions to various final fine-structure states. For comparison with experimental observations of angular distribution parameter β, the average Auger-decay anisotropy parameter α_2 for a group of unresolved Auger lines is calculated by weighting each α_2 value with the corresponding Auger rate,

$$\overline{\alpha}_2=\sum_f W_{i\rightarrow f}^T\alpha_{2_{i\rightarrow f}}/\sum_f W_{i\rightarrow f}^T. \quad (3)$$

In order to determine how different many-electron effects such as the configuration interaction in the intermediate (IISCI) and final ionic state and the exchange interaction between the bound and continuum electrons contribute to the anisotropy of the Auger process, the calculations were carried out in different approximations. In approximation FE, bound orbitals were optimized for the final ionic state and kept frozen during the Auger decay. The jj-average exchange interaction and the Lagrangian multipliers were included in the calculation of the continuum orbital. The effect of exchange interaction between the continuum and bound electrons was studied by using the same bound orbitals as in the FE calculation, but by neglecting the exchange potential in the calculation of the continuum orbitals (the approach is labeled F). The continuum orbitals were then Schmidt orthogonalized against the bound orbitals. The difference between the results F and FE thus gives an estimate of the influence of exchange interaction on the anisotropy of Auger decay. Our approach F resembles closely the method used by Chen [3].

The approximation IE is identical to FE, but the bound orbitals which were optimized for the intermediate state were also used in the construction of the final-ionic-state many-electron wave function. Comparison between the FE and IE results thus shows the influence of the choice of one-electron orbitals to the anisotropy of the decay. The approximation FEI is equivalent to FE, except that the intermediate-state mixing coefficients were obtained from the intermediate-state self-consistant-field (SCF) calculation. The difference between FE and FEI values is caused by changes in the mixing coefficients.

In Table I we give the values of the angular-distribution parameter $\beta=\alpha_2 A_{20}$ obtained in various approximations for the $3d_{5/2}^{-1}5p_{3/2}\rightarrow 4p^{-2}5p$ resonant Auger transitions of Kr. For comparison, the values reported by Chen [3] are also shown.

The $3d_{3/2}^{-1}5p$ excited state is split into two atomic states, separated by 0.031 eV according to an SCF calculation.

TABLE II. Experimental and calculated angular anisotropy parameters $\beta=\alpha_2 A_{20}$ for Kr $3d_{3/2}^{-1}5p\rightarrow 4p^{-2}5p$ Auger transitions. FE is the same as in Table I. FEI indicates the values obtained using final-state state orbitals with exchange but calculating IISCI with initial-state orbitals. FEO is the same as FE but IISCI was excluded. An asterisk indicates that experimental β's for these lines could not be determined due to their low intensity.

Final ionic state		Line	Energy (eV)	First initial state				Second initial state				
Parent	Term	in expt.	Expt.	FE	FEI	FEO	Chen [3]	FE	FEI	FEO	Chen [3]	Expt.
$4p^4(^3P)5p$	$^4P_{5/2}$	1	61.822	−0.999	−0.987	−0.957	−0.998	0.324	−0.450	−0.798	−0.879	−0.98±0.02
	$^4P_{3/2}$	2	61.777	0.527	0.536	0.563	0.839	0.509	0.464	0.526	0.820	0.61±0.02
	$^4D_{7/2}$	3	61.592	0.132	0.104	0.087	0.322	0.095	0.096	0.000	0.317	−0.42±0.13
	$^4P_{1/2}$	3		−0.033	0.133	−0.147	1.259	−0.184	−0.200	0.917	−0.229	
	$^2D_{5/2}$	4	61.556	0.473	0.289	−0.831	−0.373	−0.925	−0.986	−0.702	−0.997	
	$^2D_{3/2}$	5	61.270	−0.687	0.962	0.017	−0.382	0.939	0.777	1.073	0.677	−0.15±0.11
	$^2P_{1/2}$	6	61.180	0.560	0.704	0.300	0.832	1.085	−0.208	1.004	−0.294	−0.5±0.2
	$^4D_{5/2}$	7	61.055	−0.947	−0.947	−0.942	−0.936	−0.937	−0.941	−0.892	−0.928	0.36±0.05
	$^2P_{3/2}$	8	61.052	0.668	0.402	0.795	0.117	−0.459	−0.941	−0.003	0.752	
	$^2P_{1/2}$	9	61.049	1.114	1.045	0.639	1.013	0.973	0.943	1.001	0.989	
	$^4S_{3/2}$	10	60.856	0.835	0.632	0.915	0.713	0.930	0.929	0.841	−0.160	*
	$^4D_{3/2}$	11	60.822	−0.767	−0.675	−0.935	−0.434	0.154	−0.343	0.428	0.724	−0.47±0.02
	$^4D_{1/2}$	12	60.776	0.724	0.676	0.729	0.553	0.782	0.758	0.955	0.949	*
$4p^4(^1D)5p$	$^2F_{5/2}$	13	59.931	0.867	0.344	0.451	−0.049	−0.479	−0.179	−0.160	−0.945	−0.03±0.14
	$^2F_{7/2}$	14	59.866	−0.848	−0.844	−0.842	−0.693	−0.843	−0.844	0.000	−0.687	−0.98±0.02
	$^2P_{3/2}$	15	59.804	−0.576	−0.365	−0.465	−0.069	0.542	0.031	1.017	0.909	1.01±0.10
	$^2D_{3/2}$	16	59.557	0.872	0.742	−0.039	0.757	0.398	0.168	−0.566	−0.591	0.52±0.13
	$^2P_{1/2}$	17	59.551	0.704	0.688	0.652	0.908	0.628	0.648	0.918	0.858	
	$^2D_{5/2}$	18	59.542	−0.122	−0.573	0.481	−0.577	1.218	1.086	−0.138	1.141	
$4p^4(^1S)5p$	$^2P_{1/2}$	19	57.564	1.014	1.006	0.676	1.004	0.994	0.988	0.999	0.993	1.11±0.09
	$^2P_{3/2}$	20	57.481	−0.735	−0.802	−0.754	−0.793	−0.664	−0.707	0.233	−0.701	*

These atomic states involve a strong mixing of the $3d_{3/2}^{-1}5p_{3/2}$, $J=1$ and $3d_{3/2}^{-1}5p_{1/2}$, $J=1$ jj-coupled configurations. According to the photoexcitation probabilities predicted by the GRASP code [8], only the first one of the atomic states is remarkably populated via photoexcitation. Table II shows calculated values of the β parameters for both intermediate atomic states.

The FEI results were also reported in an earlier work [1] and argued to offer the best theoretical description. Lack of reliable experimental results made it impossible to compare experiment with theoretical estimates in detail. Present experimental results allow us to clarify whether it is possible to confirm the validity of the FEI approximation to describe the experiment.

III. EXPERIMENT

A. Measurements

The experiments were performed at the Finnish beamline (BL51) at MAX-laboratory in Lund, Sweden. A detailed description of the beamline has been published elsewhere [9,10]. Briefly, it uses synchrotron radiation from an undulator operating in the 60–600-eV photon energy range and it has a modified SX-700 plane grating monochromator with a plane elliptical focusing mirror. Recently, an end station [11] equipped with a high-resolution SES-200 hemispherical electron spectrometer [12] has been installed at the beam line. In order to facilitate the angular-distribution measurements, the spectrometer can be rotated in a plane perpendicular to the direction of the photon beam. The spectrometer is provided with a five-element retarding-accelerating lens that also allows the compensation of mechanical misalignments and small variations in the position of the source point at different analyzer angles. An ultimate energy resolution better than 14 meV (full width at half maximum) has been achieved so far, although the total linewidth in the present measurements was in the range 30–35 meV, which allowed us to resolve the different fine-structure components with reasonable intensity.

We did not determine exact numerical values for the degree of linear polarization but it can be estimated to be very high (above 99%). This can be seen as an almost complete absence of the Kr $4s$ photoelectron line in the spectrum measured at 90°. It is well known that electrons originating from s shells should have angular-distribution parameter β very close to 2 well above the ionization threshold [13].

The angular-distribution parameters were determined by measuring the resonance Auger spectra at 0°, 54.7°, and 90° with respect to the polarization plane. Transmission correction for each angle was obtained by measuring the Ne $2p$ photoelectron lines at the same kinetic-energy region using the same experimental conditions. The measured Ne $2p$ intensities were normalized using the photoionization cross sections given in Ref. [14] and the β parameters from Ref. [15].

In order to determine the β parameter experimentally for a given photoelectron or Auger line, one must in principle know the absolute electron intensities at two or more angles.

This is not a trivial task in synchrotron radiation experiments due to, e.g., rapidly decreasing photon flux, problems related to accurate flux measurement, and electromagnetic noise generated by laboratory equipment. During the present study it was observed that the spectrometer is extremely sensitive to any small changes in electron-beam position in the storage ring, especially when the spectra were recorded with very high electron-energy resolution. Related changes in the photon distribution within the source volume, from which the lens collects electrons, were also observed to change both resolution and transmission properties of the spectrometer. Thus it was not possible to obtain absolute intensity calibration with reasonable accuracy. Instead, the spectra measured at different angles were normalized by assuming β parameters for some lines to be known. The lines chosen for this purpose were the $4s$ photoelectron line ($\beta \approx 2$) and the $3d_{3/2,5/2}^{-1}5p \rightarrow 4p^4(^3P)5p \ \ ^4P_{5/2}$ resonance Auger line ($\beta \approx -1$). The final results were obtained by an iterative process in which these initial values were varied within a small range. The error limits were determined as maximum deviations from the average β's, after careful study of spectra measured under different experimental conditions. If the excited state decays via a participator process, the $4s$ photoelectron line cannot be used for normalization. According to the calculations of Ref. [1], the participator decay probability is negligible compared to the spectator decay.

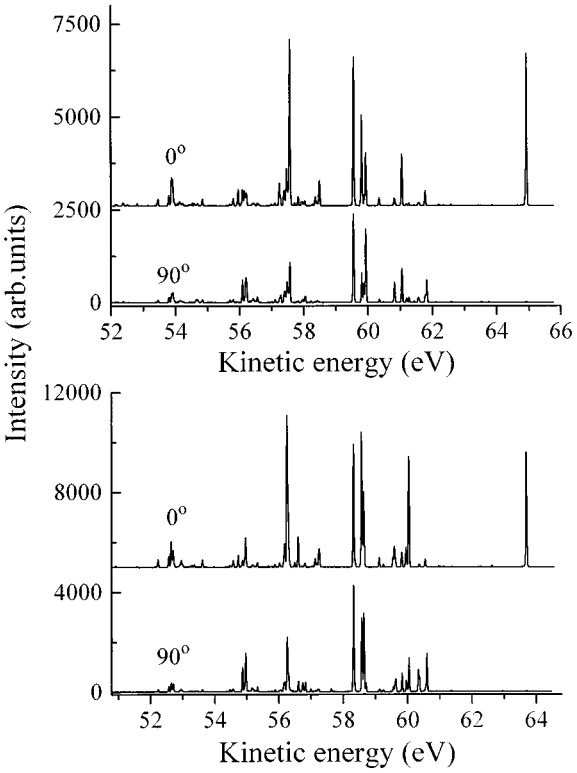

FIG. 1. Lower part: the $3d_{5/2}^{-1}5p \rightarrow 4p^45p$ resonance Auger spectrum of Kr excited by 91.200-eV photons. Upper part: the corresponding $3d_{3/2}^{-1}5p \rightarrow 4p^45p$ resonance Auger spectrum excited by 92.425-eV photons. The angle between the lens axis and the electric-field vector of incoming radiation is also shown in each spectrum.

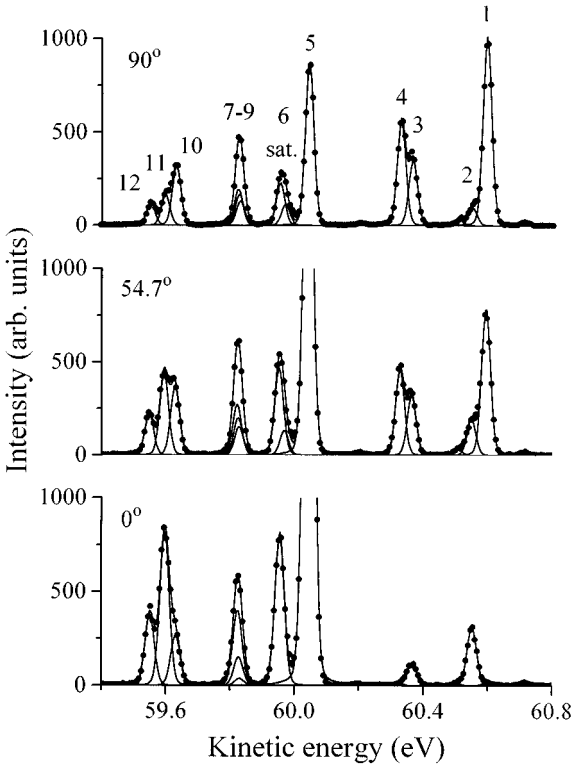

FIG. 2. Kinetic-energy region of the $3d_{5/2}^{-1}5p \rightarrow 4p^4(^3P)5p$ resonance Auger transitions measured at 0°, 54.7°, and 90°.

B. Experimental results

The resonance Auger electron spectra following the $3d_{3/2,5/2} \rightarrow 5p$ resonant excitations, measured at 0° and 90°, are displayed in Fig. 1. In order to determine the relative line intensities at each angle, the spectra were least squares fitted using Voigt functions. The energy positions were kept fixed and the line shapes were constrained to be the same for all lines within a spectrum. It must be pointed out that the use of Voigt line shapes may be somewhat inadequate since Aksela *et al.* showed recently that the shape of a resonance Auger line is given as a product (and not as a convolution) of photon energy distribution and Lorentzian lifetime width [16]. The curve fitting results for the $3d_{5/2}^{-1}5p \rightarrow 4p^4(^3P)5p$ spectator transitions measured at 0° and 90° are displayed in Fig. 2 and the corresponding results for the $4p^4(^1D)5p$ final states in Fig. 3. Figures 4 and 5 show the same final states following the $3d_{3/2} \rightarrow 5p$ excitation. The obtained β parameters are summarized in Tables I and II together with the calculated values.

Kinetic-energy calibration was made with the aid of the photoexcitation energies of King *et al.* [17] (91.200 eV and 92.425 eV for $3d_{5/2} \rightarrow 5p$ and $3d_{3/2} \rightarrow 5p$ excitations, respectively). The final-state binding energies were obtained from the optical energy levels of Moore [18]. Photoelectron satellite lines accompanying the direct $4s$ photoionization channel were also taken into account using the line positions from Ref. [19]. Although the $4s$ satellites are in general much weaker than the resonance Auger lines, they can affect the analysis considerably, especially when the β parameter for a close-lying resonance Auger line is close to 2 or -1, i.e., the line almost vanishes at the extreme angles.

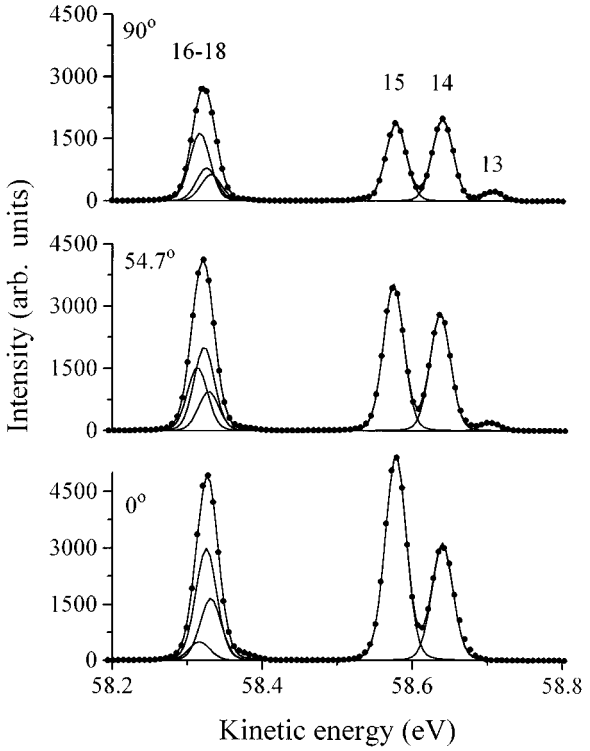

FIG. 3. Kinetic-energy region of the $3d_{5/2}^{-1}5p \rightarrow 4p^4(^1D)5p$ resonance Auger transitions measured at 0°, 54.7°, and 90°.

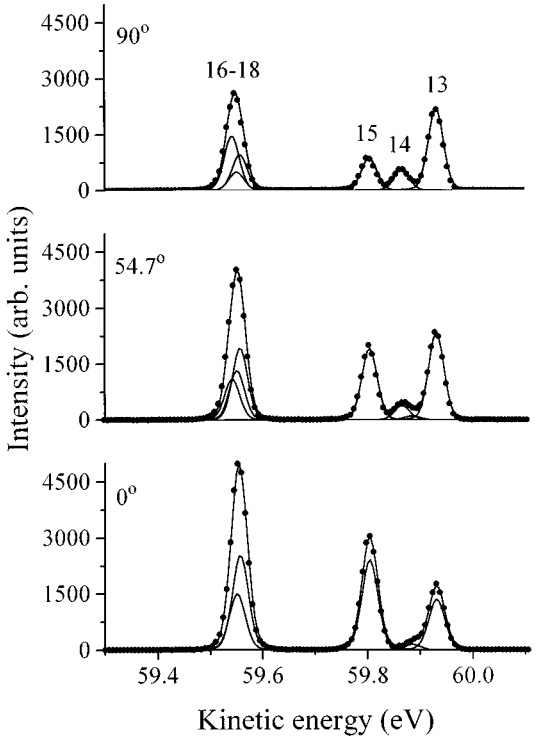

FIG. 5. Kinetic-energy region of the $3d_{3/2}^{-1}5p \rightarrow 4p^4(^1D)5p$ resonance Auger transitions measured at 0°, 54.7°, and 90°.

Concerning the $3d_{5/2}^{-1}5p \rightarrow 4p^4(^3P)5p$ transitions, lines 1 and 4 must have very negative β parameters since both of them are hardly visible in the 0° spectrum. Thus our initial guess that line 1 has $\beta \approx -1$ is reasonable. Line 2 is accompanied on its low-energy side by a $4s$ satellite, thus hampering its accurate intensity determination. A similar situation occurs in the case of lines 5 and 6 where two additional $4s$ satellites overlap with them and the separation of resonant contribution from the nonresonant part is by no means clear. It is easy to see, however, that line 5 must have a large positive β parameter since its intensity is strongly enhanced at 0°. Lines 7, 8, and 9 are located at approximately 6 meV. Although these lines were fitted separately, we made no attempts to get individual asymmetry parameters for them. Again, one $4s$ satellite line overlaps with this group. Lines 10 to 12 are hardly separated from each other. Because line 11 obviously has largely positive β, it almost prevents the determination of intensity for line 10, whose intensity is nearly angle independent. The same arguments are mostly valid in the case of the $3d_{3/2}^{-1}5p \rightarrow 4p^4(^3P)5p$ transitions. We were not able to determine β's for lines 10, 12, and 20 with reasonable accuracy, either because of their low intensity or because of uncertain $4s$ satellite contribution.

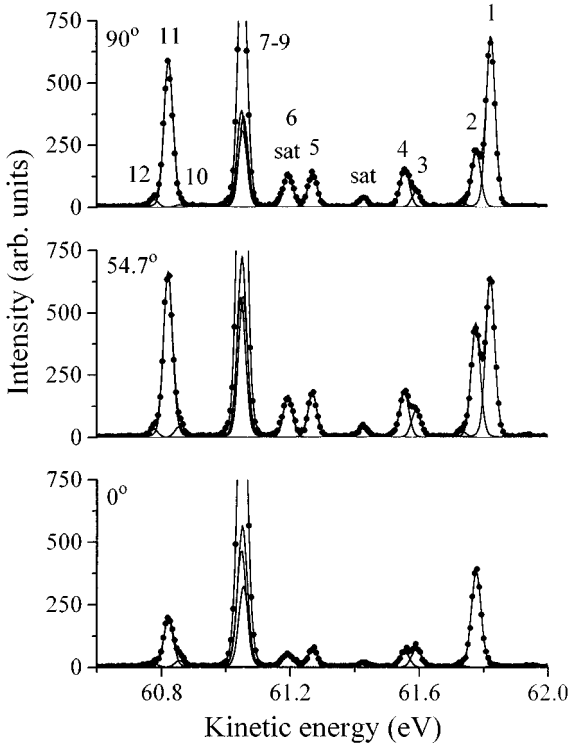

FIG. 4. Kinetic-energy region of the $3d_{3/2}^{-1}5p \rightarrow 4p^4(^3P)5p$ resonance Auger transitions measured at 0°, 54.7°, and 90°.

There are six final states within the $4p^4(^1D)5p$ parent (lines 13–18). Three of them (16–18) are again too close to each other to allow separate β parameters to be determined. Line 13 has very low intensity at the $3d_{5/2}^{-1}5p$ resonance, which makes its intensity analysis very difficult. At the $3d_{3/2} \rightarrow 5p$ excitation the situation is different for this parent. Then line 13 gains considerable intensity but line 14 disappears at 0°. The shoulder in the low kinetic-energy side of line 13 is most probably a $4s$ satellite line.

The ^1S parent is split into two components, $^2P_{1/2}$ and $^2P_{3/2}$. Of these, only the latter is populated at the $3d_{5/2}^{-1}5p$ resonance. This line is located at such a low kinetic energy that the $4p^4(^3P)6p$-type shakeup final states overlap with it.

TABLE III. Intensity-weighted sums of β coefficients for Kr $3d_{5/2}^{-1}5p \rightarrow 4p^4 5p$ Auger transitions. Computational approximations IE, F, FE, and FEI have been explained in the text. Line numbers refer to Table I. The labeling of peaks in the leftmost column refers to [5,6].

Peak	Lines	Theory						Experiment		
	included	IE	F	FE	FEI	Ref. [2]	Ref. [3]	Ref. [6]	Ref. [5]	This work
1a	1, 2	−0.793	−0.567	−0.540	−0.535	−0.990	−0.66	−0.76(2)	−0.89	−0.64
1b	3, 4	−0.668	−0.925	−0.778	−0.773	−0.823	−0.88	−0.87(2)	−0.98	-0.78
1c	5, 6	0.894	0.784	0.699	0.705	0.801	0.83	0.77(6)	0.62	1.00
1d	7–9	0.792	−0.368	−0.309	−0.338	0.820	−0.12	0.04(5)	0.24	0.07
1e	10–12	0.444	0.452	0.268	0.277	0.467	0.42	0.31(6)	0.19	0.56
2a	13–15	0.128	0.116	0.240	0.247	−0.066	0.12	0.27(3)	−0.06	0.41
2b	16–18	−0.457	−0.011	0.048	0.043	−0.248	−0.06	0.05(3)	−0.12	0.24
4	20	0.807	0.835	0.795	0.825	0.759	0.84		0.73	0.86

We have assumed that the most intense line in this energy region is the $4p^4(^1S)5p\ ^2P_{3/2}$ resonance Auger line, but due to heavy overlap of lines this interpretation is nevertheless somewhat uncertain. In the case of the $3d_{3/2}^{-1}5p$ resonance both components are populated but now the transitions to the $4p^4(^1S)5p\ ^2P_{1/2}$ final states are more intense.

Present experimental β values are compared with the previous experimental results of Caldwell [6] and Carlson *et al.* [5] in Tables III and IV. The results are in reasonable agreement with each other, although in some cases the scattering in β parameters is very large. Since some important β's were not presented in Ref. [6] (peak 4) we cannot definitively discuss the origin of the discrepancies. Some notes about the importance of resolution can be made, however. The photon- and electron-energy resolutions in Ref. [5] were 0.37 eV and 0.12 eV, respectively. This level of resolution only allowed clear separation of the ^1D and ^3P parent multiplets but fine structures within them remained mostly unresolved. Caldwell cited (50 ± 3)-meV photon- and (80 ± 5)-meV electron-energy resolution in Ref. [6], which was sufficient to separate some of the daughter levels inside the parents. Many of the observed peaks still contained more than one transition.

IV. DISCUSSION

A. Comparison between experiment and theory

Calculated and in most cases also the experimental angular anisotropies given in Tables I and II refer to transitions between each individual initial and final state. For several transitions in the $3d_{5/2}^{-1}5p_{3/2}$ spectrum (Table I) the agreement between experiment and theory is excellent. Among these transitions there are several lines for which the β parameters are only very weakly sensitive to the details of theoretical calculations. The transitions to the $4p^4(^3P)5p\ ^4P_{5/2}$ state (line 1) and the $4p^4(^3P)5p\ ^2D_{5/2}$ state (line 4) serve as excellent examples here. Insensitivity of β values can be traced back to the fact that both lines are strongly dominated by the $\epsilon d_{5/2}$ transition amplitudes. The effect of the exchange interaction would be seen as the difference between the F and FE results. The choice of the one-electron orbitals would show up when comparing the FE and IE values to each other. These correlation effects, however, only result in a scaling of the transition amplitudes in Eq. (2) by a constant factor. The common scaling factor of the partial amplitudes is then normalized out when the β parameters are determined. The FISCI, predicted by initial- or final-state orbitals, may result in a change in the eigenvector decomposition between the two final states. The transitions to both of the jj-coupled states that are of major importance in the many-electron wave function for lines 1 and 4 are dominated by the same transition amplitude and characterized by the same (practically geometrical) β value. The angular anisotropy thus remains insensitive also to the FISCI. The dominance of the $\epsilon d_{5/2}$ partial wave is assumed to make the β parameters of lines 1 and 4 insensitive to the final-continuum-state configuration interaction (FCSCI) as well [7].

In the case where only one partial wave is strongly dominating, the angular anisotropy parameter is in practice given by a geometrical quantity. Since the alignment of the excited state is also known, such transitions can be used for calibration purposes. Our choice to use line 1 as a calibration line with known β is thus well supported by present calculations. The angular anisotropies predicted by theory for lines that are of similar character (see below) are in a good agreement with the experimental values. This confirms that the transmission correction using the Ne $2p$ photoelectron lines is reliable.

Besides lines 1 and 4, the $3d_{5/2}^{-1}5p_{3/2}$ spectrum consists of several transitions where the calculated anisotropy is only very weakly sensitive to the details of the theoretical description. The transitions to the $J=5/2$ final state (lines 13 and 18) have the $\epsilon d_{5/2}$ partial wave as the dominating one. The final states are mixtures of some jj-coupled states. Mixing does not alter the β values considerably since all the transitions are within the jj-coupling scheme characterized by largely negative β values. Therefore, the β values for lines 13 and 18 vary only slightly in different approximations. The same holds true also for the transition to the final $4p^4(^1S)5p\ ^2P_{3/2}$ state (line 20), which is governed by the $\epsilon d_{5/2}$ partial wave. The other final states with $J=3/2$ have large $\epsilon d_{3/2}$ and $\epsilon d_{5/2}$ partial amplitudes, but because these waves have a very small phase difference the phase factor $\Delta_{\kappa\kappa'}$ in Eq. (2) is close to 1. The changes in β values are therefore in most cases fairly small. Agreement between experiment and theory is reasonable for most of the states with $J=3/2$, which can be resolved in experiment. For lines 2, 5, and 11 all the calculations estimate the β values primarily from geometrical quantities and the agreement with experiment is good as expected.

TABLE IV. Intensity-weighted sums of β coefficients for Kr $3d_{3/2}^{-1}5p \rightarrow 4p^4 5p$ Auger transitions. The approximations FE and FEI are explained in the text. The different values of peak 2a in Ref. [6] originate from two different experiments. Line numbers refer to Table II. The labeling of peaks in the leftmost column refers to [5,6].

Peak	Lines	Theory			Experiment		
	included	FE	FEI	Ref. [21]	Ref. [6]	Ref. [5]	This work
1a	1, 2	−0.656	−0.476	−0.002	−0.45(7)	−0.48	−0.32
1b	3, 4	0.126	0.077	−0.159	−0.18(17)	−0.20	−0.12
1c	5, 6	0.249	0.871	0.870	−0.50(9)	0.46	−0.32
1d	7–9	−0.557	−0.237	−0.902	0.15(10)	0.14	0.36
1e	10–12	−0.330	−0.516	0.781	−0.41(8)	−0.26	−0.36
2a	13–15	−0.292	−0.079	−0.264	−0.42(6),0.43(15)	−0.16	0.32
2b	16–18	0.331	0.320	0.140	0.24(7)	0.08	0.52
4	19–20	−0.243	0.386	0.030		0.49	1.11

Line 10 in experiment, for which the theory seems to overestimate the anisotropy, is due to the transition to the $4p^4(^3P)5p\ ^4S_{3/2}$ final state, which is strongly mixed with the $4p^4(^3P)5p\ ^4D_{3/2}$ state (line 8). Here the mixing combines transitions characterized by somewhat different β values. The discrepancy between experiment and theory for line 10 thus indicates that the eigenvectors, especially in the case of lines 8 and 10, are not properly predicted by the calculations. A similar situation occurs in the case of lines 15 and 16. The final state $4p^4(^1D)5p\ ^2P_{3/2}$ of transition 15 is mixed with the final state $4p^4(^1D)5p\ ^2D_{3/2}$ (line 16). The mixing is not correctly predicted by any of the calculations. As seen from Table I, the β of line 16 is also sensitive to FISCI. The variations are even larger than in the case of line 15. Since lines 16, 17, and 18 are not resolved, it is hard to say whether FE or IE is in better agreement with experiment.

Most interesting are the transitions with several more or less equally contributing channels. Both the $\epsilon d_{5/2}$ and $\epsilon g_{9/2}$ amplitudes are large in the case of the transition to the $4p^4(^3P)5p\ ^4D_{7/2}$ state. Unfortunately, this line overlaps strongly with a line which is due to the transition to the $4p^4(^3P)5p\ ^4P_{1/2}$ state (line 3), and the validity of different calculations cannot be tested. The transition to the $4p^4(^1D)5p\ ^2F_{7/2}$ (line 14) state is again strongly dominated by the $\epsilon g_{9/2}$ partial amplitude. Even though this amplitude has been found to be very sensitive to the exchange interaction, the β value is less sensitive. The result obtained with exchange, however, seems to reproduce the experiment slightly better here. For weak lines or for lines where the individual transitions cannot be resolved, the comparison between experiment and theory is less reliable. This holds for most of the lines with $J=1/2$.

In the case of the $3d_{3/2}^{-1}5p$ spectrum, the ISCI plays a prominent role. There are very few lines which are weakly sensitive both to the initial- and the final-state effects. One of them is line 2, for which all the predictions agree reasonably well with experiment. The second one is line 19, for which the experimental β value is also well reproduced by all the calculations. Other lines that are only weakly influenced by ISCI are not well enough resolved in the experiment.

For most of the lines in the $3d_{3/2}^{-1}5p$ spectrum, the ISCI is of great importance. In such cases the β parameters depend critically on the method to account for ISCI. This can be seen from large variations between the FE, FEI, and FEO results in Table II. Comparison with experiment indicates that the biggest problems in the theory of angular anisotropy are connected to the difficulties to correctly account for ISCI. On the other hand, just as in the case of the $3d_{5/2}^{-1}5p$ transitions, the β parameter is found to be insensitive to the exchange interaction. The $4p^4(^1D)5p\ ^2F_{7/2}$ line especially, where the exchange plays the most prominent role, but where the β values are hardly affected whether the exchange is included or not, allows this kind of conclusion.

B. General

In a recent study [20], electron correlation was studied by carrying out a detailed comparison between the experimental and calculated partial transition rates. Exchange interaction was observed to be of large importance in the intensity ratios [20]. In this work, the angular anisotropy has been obtained to be fairly insensitive to exchange interaction. On the other hand, FISCI affects both the partial rates and the angular parameters in a similar way. If the jj-coupled states with similar β values are mixed, the anisotropy cannot be used to test the capacity of the MCDF calculations to account for FISCI. In a few cases the testing becomes possible. As a result of the present study we conclude that FISCI is not well enough described by present MCDF calculations. This is in agreement with the previous study on partial rates [20], where for some states with $J=3/2$ the theory was unable to reproduce the experiment.

In the case of the $3d_{3/2}^{-1}5p$ transitions, the ISCI plays a very important role, but the calculations are not capable of reproducing it correctly. Inspection of Table IV, where the intensity-weighted sums of β parameters are given, indicates that the best theoretical description so far for the $3d_{3/2}^{-1}5p$ transitions is provided by the FEI calculations.

Next we will shortly compare the present experimental results with previous studies [5,6]. We have retained the same peak labeling used in the other works in order to make the comparison easier. In most cases it is only one of the lines in each peak of Tables III and IV that has strong anisotropy. This may be the main reason why previous results of lower resolution are in satisfactory agreement with present ones. Despite the fact that our resolution is superior as compared to that of Refs. [5,6], most of the peaks retain their character. For example, all authors report large negative β

values for peaks 1a and 1b in Table III and for peaks 1a, 1c, and 1e in Table IV. In general, our values tend to be closer to those of Ref. [6].

The improved experimental accuracy does not always provide essentially better tools to study the effects related to angular anisotropy if the anisotropy of several lines coalescing into a peak is small. Better resolution, however, allows us to confirm that for some transitions the β values are determined by geometrical quantities as foreseen by theory. Resolving such lines from experiment helps to make use of their known β's for the calibration purposes.

According to Eq. (3) the average angular anisotropy parameters involve the partial transition rates. The latter ones are influenced, e.g., by exchange interaction in a more sensitive way as compared to the individual β values. The average β values may thus be considered as a useful test to the theory as well. This holds true especially in cases where some individual β parameters in an average value are merely given by geometrical quantities where the quality of wave functions plays no role.

V. CONCLUSIONS

High resolution has made it possible, for the first time, to determine most of the individual β values of the Kr $3d^{-1}_{3/2,5/2}5p \rightarrow 4p^{-2}5p$ transitions and to compare them with theory. The angular anisotropy parameters of some transitions are in practice given by geometrical quantities which offers a calibration method for the experiment.

The individual β values of some transitions are extremely sensitive to ISCI and FISCI, but so are the partial transition rates and energy splittings [1,20]. This means that all three quantities are needed for a comparison between experiment and theory. All results are important when the aim is to arrive at a better description of the electron correlation effects. Recent high-resolution experimental results for intensities and energies [20] combined with the β's of this work and the theorical analysis given here will thus serve as a starting point for future work in improving the theory.

ACKNOWLEDGMENTS

The staff of MAX-laboratory as well as Dr. O.-P. Sairanen, E. Kukk, and J. Karvonen are acknowledged for assistance during the measurements. Dr. J. Tulkki and Dr. N. M. Kabachnik are acknowledged for their contributions in the earlier stage of the theoretical work. This work has been supported by the Research Council for the Natural Sciences of the Academy of Finland, the Knut and Alice Wallenberg Foundation in Sweden, and the Swedish Natural Science Research Council (NFR).

[1] J. Tulkki, H. Aksela, and N. M. Kabachnik, Phys. Rev. A **50**, 2366 (1994).
[2] U. Hergenhahn, B. Lohmann, N. M. Kabachnik, and U. Becker, J. Phys. B **26**, L117 (1993).
[3] M. H. Chen, Phys. Rev. A **47**, 3733 (1993).
[4] G. S. Brown, M. H. Chen, B. Crasemann, and G. E. Ice, Phys. Rev. Lett. **45**, 1937 (1980); G. B. Armen, T. Åberg, J. C. Levin, B. Crasemann, M. H. Chen, G. E. Ice, and G. S. Brown, *ibid.* **54**, 1142 (1985); A. Kivimäki, A. Naves de Brito, S. Aksela, H. Aksela, O.-P. Sairanen, A. Ausmees, S. J. Osborne, L. B. Dantas, and S. Svensson, *ibid.* **71**, 4307 (1993).
[5] T. A. Carlson, D. R. Mullins, C. E. Beall, B. W. Yates, J. W. Taylor, D. W. Lindle, B. P. Pullen, and F. A. Grimm, Phys. Rev. Lett. **60**, 1382 (1988); T. A. Carlson, D. R. Mullins, C. E. Beall, B. W. Yates, J. W. Taylor, D. W. Lindle, and F. A. Grimm, Phys. Rev. A **39**, 1170 (1989).
[6] C. D. Caldwell, in *X-Ray and Inner-Shell Processes*, edited by T. A. Carlson, M. O. Krause, and S. T. Manson, AIP Conf. Proc. No. 215 (AIP, New York, 1990), p. 685.
[7] J. Tulkki, N. M. Kabachnik, and H. Aksela, Phys. Rev. A **48**, 1277 (1993).
[8] K. G. Dyall, I. P. Grant, C. T. Johnson, F. A. Parpia, and E. P. Plummer, Comput. Phys. Commun. **55**, 425 (1989).
[9] S. Aksela, A. Kivimäki, A. Naves de Brito, O.-P. Sairanen, S. Svensson, and J. Väyrynen, Rev. Sci. Instrum. **65**, 831 (1994).
[10] S. Aksela, A. Kivimäki, O.-P. Sairanen, A. Naves de Brito, E. Nõmmiste, and S. Svensson, Rev. Sci. Instrum. **66**, 1621 (1995).
[11] S. Svensson J.-O. Forsell, H. Siegbahn, A. Ausmees, G. Bray, S. Södergren, S. Sundin, S. J. Osborne, S. Aksela, E. Nömmiste, J. Jauhiainen, M. Jurvansuu, W. R. Salaneck, A. Evaldsson, M. Lögdlund, and A. Fahlman, Rev. Sci. Instrum. (to be published).
[12] N. Mårtensson, P. Baltzer, P. A. Brühwiler, J.-O. Forsell, A. Nilsson, A. Stenborg, and B. Wannberg, J. Electron Spectrosc. Relat. Phenom. **70**, 170 (1994).
[13] H. Derenbach and V. Schmidt, J. Phys. B **17**, 83 (1984).
[14] J. M. Bizau and F. J. Wuilleumier, J. Electron Spectrosc. Relat. Phenom. **71**, 205 (1995).
[15] V. Schmidt, Z. Phys. D **2**, 275 (1986).
[16] S. Aksela, E. Kukk, H. Aksela, and S. Svensson, Phys. Rev. Lett. **10**, 1917 (1995).
[17] G. C. King, M. Tronc, F. H. Read, and R. C. Bradford, J. Phys. B **10**, 2479 (1977).
[18] C. E. Moore, *Atomic Energy Levels*, Natl. Bur. Stand. (U.S.) Circ. No 467 (U.S. GPO, Washington, D.C., 1952), Vol II.
[19] A. Kikas, S. J. Osborne, A. Ausmees, S. Svensson, O.-P. Sairanen, and S. Aksela, J. Electron Spectrosc. Relat. Phenom. (to be published).
[20] H. Aksela, J. Jauhiainen, E. Kukk, E. Nõmmiste, S. Aksela, and J. Tulkki, Phys. Rev. A **53**, 290 (1996).
[21] U. Hergenhahn, B. Lohmann, N. M. Kabachnik, and U. Becker, J. Phys. B **24**, 4759 (1991).